Article

The Formation of Strong {100} Texture by Dynamic Strain-Induced Boundary Migration in Hot Compressed Ti-5Al-5Mo-5V-1Cr-1Fe Alloy

Kai Li and Ping Yang * ID

School of Materials Science and Engineering, University of Science and Technology Beijing, Beijing 100083, China; likai09260926@126.com
***** Correspondence: yangp@mater.ustb.edu.cn; Tel.: +86-010-8237-6968

Abstract: The microstructure and texture evolution of Ti-5Al-5Mo-5V-1Cr-Fe alloy during hot compression were investigated by the electron backscatter diffraction technique. The results reveal that two main texture components containing <100> and <111> fiber textures form after the hot compression. The fraction of each component is mainly controlled by deformation and strain rate. Dynamic strain-induced boundary migration (D-SIBM) is proved to be the reason that <100>-oriented grains grow towards <111>-oriented grains. The <100>-oriented grains coarsen with the increasing <100> texture intensity. Dynamic recrystallization (DRX) occurs under a low strain rate and large deformation. The DRX grains were detected by the method of grain orientation spread. The DRX grains reserve a <100> fiber texture similar to the deformation texture; however, DRX is not the main reason causing the formation of a strong <100> texture, due to its low volume fraction.

Keywords: hot compression; dynamic recovery; dynamic recrystallization; texture

1. Introduction

Titanium and titanium alloys are widely used for aviation, aerospace, marine, and other special applications owing to their low density, high strength, and good fatigue and corrosion performance. Thermomechanical processing is usually used for titanium alloys to improve their mechanical properties by changing their microstructure. The microstructure and mechanical properties of titanium alloys are sensitive to processing parameters such as deformation temperature and strain rate [1,2]. The hard processing characterization of titanium alloy is also a problem during industrial manufacture [3]. Many titanium alloys are hot processed in the β single region to obtain a homogeneous microstructure.

Textures of the β phase in many titanium alloys have been investigated by many researchers [4–6]. Different texture components occur under different processing parameters, and the evolution of texture would determine the mechanical properties of titanium alloys [7]. Kou et al. [8] revealed the texture revolution of Ti-15Mo-3Al-2.7Nb-0.2Si alloy during hot rolling. With increasing rolling reduction, the texture of the sample changed evidently and the final texture of rolling was a weak Goss texture in the β phase. Kim et al. [9] obtained a well-developed {001} <110> texture in Ti-22Nb-6Ta alloy under cold rolling and heat treatment at 873 K, and a {112} <110> recrystallization texture was developed after the heat treatment at 1173 K. Some specific textures may cause heterogeneity or poor fatigue performance; as a result, revealing the regularity of texture evolution for controlling its production is apparently important. Previously, we studied a strong <100> texture in Ti-5Al-5Mo-5V-1Cr-1Fe forged bar, illustrating that repeated recovery caused by the formation of large <100>-oriented grains [10].

Dynamic recovery of the β phase is quite common during hot deformation, and recrystallization occurs under some special deformation processes [11,12]. Dynamic recrystallization of a hot-rolled

titanium and its effects were studied by Chen et al. [13]. They concluded that the weakening of the texture was associated with the rotation of the dynamic recrystallization grains towards the preferred slip systems, leading to large misorientations between them. The texture of dynamically recovered β phase differs greatly from the dynamic recrystallization β phase. Li et al. [14] studied the effect of dynamic restoration on texture evolution. A strong <001> fiber texture develops where only dynamic recovery (DRC) occurs, and the deformation texture is weakened to a large extent after recrystallization. The texture of compressed molybdenum always has a similar characteristic with β titanium, because of the same body-centered cubic structure. Sophie et al. [15] observed strong <100> fiber texture and <111> fiber texture in compressed samples, and the volume fraction of <100> texture increased with increasing true strain and deformation temperature. Although the dynamic recovery and dynamic recrystallization during hot deformation have been investigated by various techniques, the effect of each mechanism on texture evolution remains unclear. Moreover, the formation of strong <100> fiber texture under a low strain rate and high deformation temperature needs to be revealed from its microstructure evolution.

This study focused on investigating the growth mechanism of <100>-oriented grains from low strain to high strain. The orientation characterizations of Ti-5Al-5Mo-5V-1Cr-1Fe alloy under different strain rates and compression temperatures were studied by the electron backscatter diffraction (EBSD) technique. The dynamic recrystallization grains were selected by the grain orientation spread (GOS) method to reveal the effect of dynamic recovery and recrystallization on texture evolution.

2. Materials and Experimental Procedures

The Ti-5Al-5Mo-5V-1Cr-1Fe alloy used in this study was obtained from a hot forged bar with a diameter of 350 mm. The composition of the alloy was 5.23 Al, 4.85 Mo, 4.93 V, 0.92 Cr, 1.17 Fe, and balance Ti. The β → α + β transus temperature of Ti-5Al-5Mo-5V-1Cr-1Fe was approximately 1143 K.

Cylindrical samples 6 mm in diameter and 12 mm in height were manufactured from the as-received Ti-5Al-5Mo-5V-1Cr-1Fe titanium bar. Before compression, each sample was heated to 1223 K and held for 5 min to obtain homogeneous β phase grains. The compression was accomplished using a Gleeble-1500 machine (DSI, St. Paul, MN, USA). The heating method was resistance heating with thermocouple to measure the temperature. And there was weak temperature fluctuation during the compression. The strain rates were $0.01~\text{s}^{-1}$, $0.1~\text{s}^{-1}$, $1~\text{s}^{-1}$ and the height reductions were 20%, 40%, 60%, and 80%. All the samples were quenched by water to retain the deformed microstructure, except those which were slowly cooled to achieve recrystallization. Two other samples under 60% compression with $1~\text{s}^{-1}$ at 1153 K were slowly cooled by 1 K/s to obtain static recrystallization.
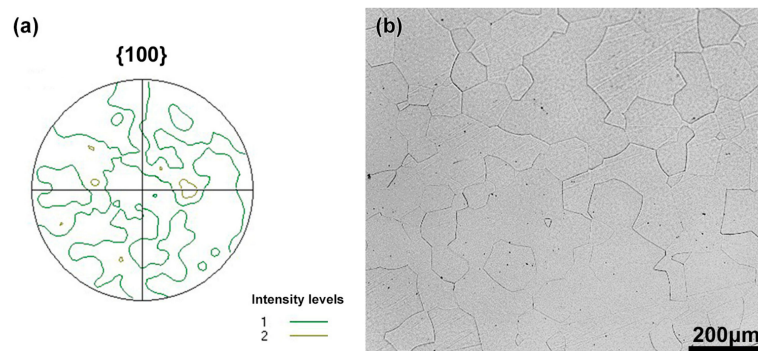
The section along and perpendicular to the compressing direction (CD) of the compressed samples was prepared for microstructure and texture determination. For EBSD examination (Oxford Instruments, London, UK), the samples were electropolished with a polishing solution of 5% perchloric acid and 95% ethyl alcohol using at 30 V for 30 s at room temperature. An EBSD system (Channel 5), mounted on an Ultra55 scanning electron microscope (ZEISS, Oberkochen, Germany), was applied to reveal the orientation feature and texture evolution under compression. The work distance for the EBSD test was 16 mm. The tested area was about 2 mm × 1.5 mm and the number of pixels was about 120,000 for each samples. The recrystallization grains were determined through the GOS method, which shows the orientation spread of all the grains. They were considered recrystallization grains once the GOS reached below 2°.

3. Results and Discussions

3.1. Initial Microstructure

There is no strong texture component in the as-received forged Ti-5Al-5Mo-5V-1Cr-1Fe alloy bar (forged 10 times around the transus point, with α + β two phases), shown in the {100} pole figure in
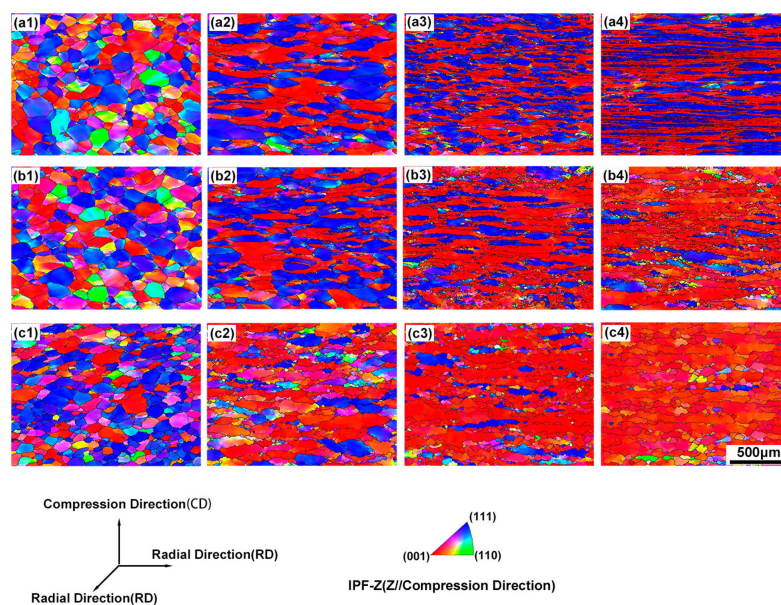
Figure 1a. The microstructure of Ti-5Al-5Mo-5V-1Cr-1Fe alloy after being held at 1223 K for 5 min is shown in Figure 1b. The initial grains of the alloy are equiaxed with a size in the range of 80–100 µm.
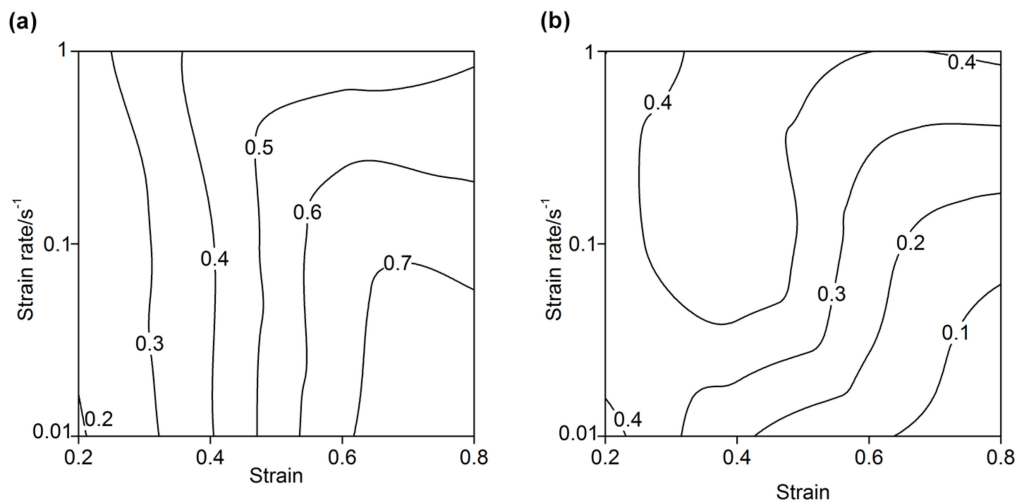

Figure 1. {100} Pole figure (**a**) of the as-received Ti-5Al-5Mo-5V-1Cr-1Fe alloy bar and original microstructure; (**b**) after solution treatment.

3.2. Texture Evolution during Hot Compression

Deformation parameters including the strain and strain rate exert an important effect on the texture components during hot compression around β transus temperature. Figure 2 shows the EBSD test results of the samples compressed at different strain rates of 1 s^{-1}, 0.1 s^{-1}, and 0.01 s^{-1} by reductions of 20%, 40%, 60%, and 80% at 1153 K. Figure 3 shows the fractions of two main fiber textures including <100> and <111> fiber textures. The two main texture components of the sample with 1 s^{-1} strain rate nearly retained the same volume fraction after 40% compression. The intensity of the <100> fiber texture increased with decreasing strain rate. In particular, the sample compressed with 80% reduction under 0.01 s^{-1} strain rate only showed <100> texture. Thus, it can be deduced that at the initial stage of compression, the strain rate has a weak effect on the texture evolution. With increasing deformation, low strain rate may be beneficial for the development of <100> texture, and <111> texture gradually weakened or even vanished.

Figure 2. Orientation maps with IPF (inverse pole figure) colors by EBSD (electron backscatter diffraction) under different parameters: (**a**1)–(**a**4) are under 1 s^{-1} with 20%, 40%, 60%, and 80% reduction; (**b**1)–(**b**4) are under 0.1 s^{-1} with 20%, 40%, 60%, and 80% reduction; (**c**1)–(**c**4) are under 0.01 s^{-1} with 20%, 40%, 60%, and 80% reduction; the compressing temperature is 1153 K.
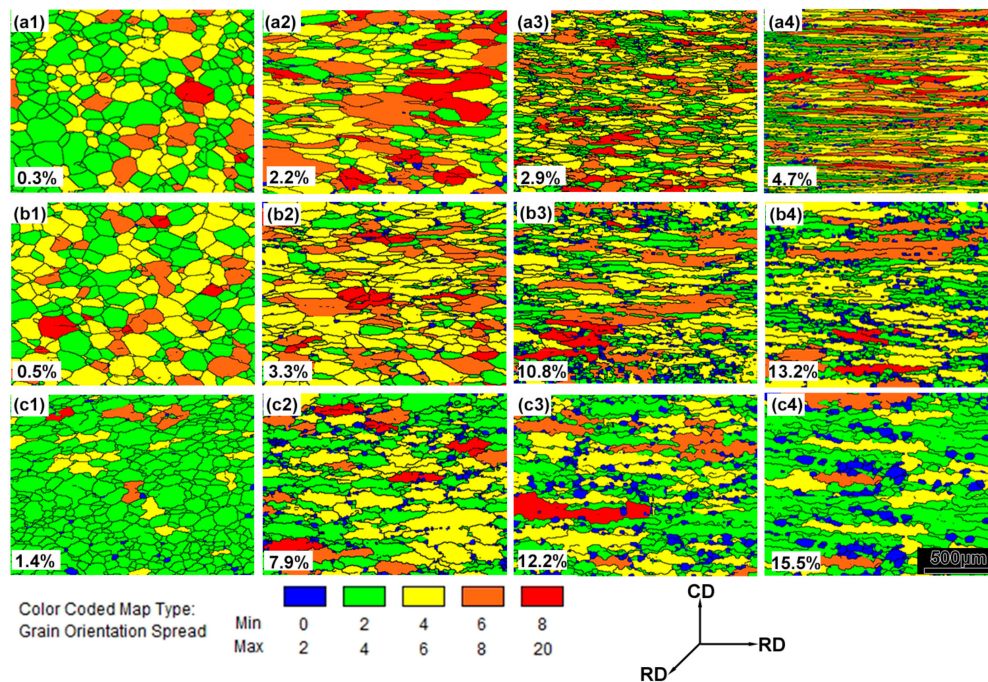
Figure 3. Fractions of <100> and <111> fiber textures under different strains and strain rates corresponding to Figure 2, the compressing temperature is 1153 K: (**a**) <100> fraction distribution; (**b**) <111> fraction distribution.
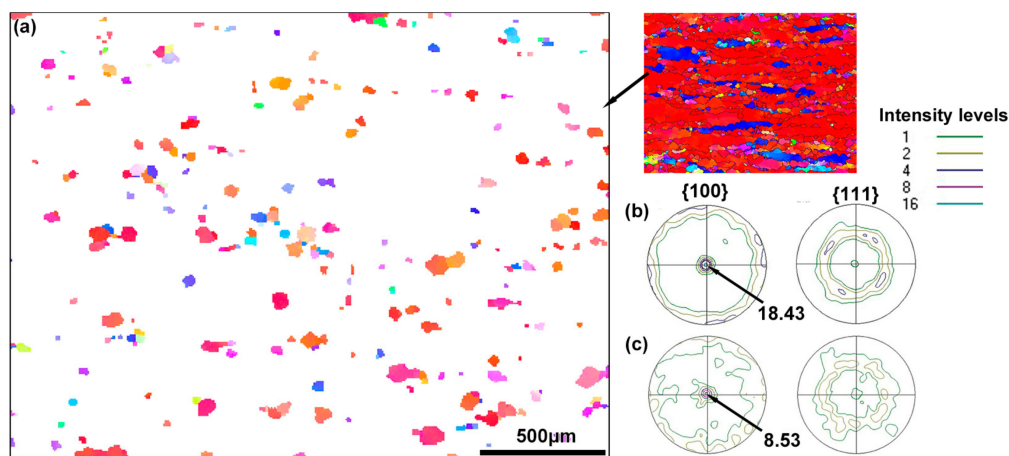
3.3. Dynamic Recrystallization during Hot Compression

Dynamic recrystallization has an important effect on the microstructure and texture evolution during hot compression. Li et al. [14] considered that DRX (dynamic recrystallization) enhanced with increasing strain rate as the dislocations accumulate rapidly, providing sufficient driving force for the transformation of the low angle boundaries into the high angle boundaries. Dynamic recrystallization grains under different compressing parameters were selected through the GOS value [16,17]. It is identified that the GOS of the recrystallized grains are below 2°. The EBSD mappings ranking the GOS of the samples corresponding to Figure 2 are shown in Figure 4. At higher strain rate, dynamic recrystallization could hardly happen and the microstructure of the samples is in the completely deformed state. The volume fraction of dynamic recrystallization distinctly rises with increasing deformation and decreasing strain rate. As recrystallization is a time-consuming process, the time is not enough for dynamic recrystallization under the condition of high strain rate. The size of the recrystallized grain is larger in lower strain rate compressed samples than in higher strain rate compressed samples. Figure 5 shows the orientation characterization of the recrystallization grains. The nucleation of dynamic recrystallization is almost located at <100>-oriented grain boundary. The misorientation inside the <100>-oriented grains increases with the rotation of each grain during compression. After full recovery, the dislocations in the <100>-oriented grains tangle together and sub-grains form inside the grains with the accumulation of dislocation clusters. Sub-grains at the grain boundary begin to grow, and their deviation from the original grain increases further and some nucleation of dynamic recrystallization then forms at the grain boundary. The recrystallized grains generate from the <100>-oriented grains and, as a result, the new dynamic recrystallized grains present a <100> recrystallization texture inherited from the initial texture. However, the <100> texture intensity is lower than the compressed grains which have not recrystallized. The dynamic recrystallization proportion in sample c4 has an obvious increase compared to other samples, and the dynamic recrystallization grain fraction is only 15.5%. As a result, dynamic recrystallization is beneficial for the formation of <100> fiber texture to a certain extent; however, it is not the main reason for this formation because of its low volume fraction.

Figure 4. Grain orientation spread of the samples with different parameters: (**a**1)–(**a**4) are under 1 s^{-1} with 20%, 40%, 60%, and 80% reduction; (**b**1)–(**b**4) are under 0.1 s^{-1} with 20%, 40%, 60%, and 80% reduction; (**c**1)–(**c**4) are under 0.01 s^{-1} with 20%, 40%, 60%, and 80% reduction; the compressing temperature is 1153 K; the blue grains are selected as the recrystallization grains.
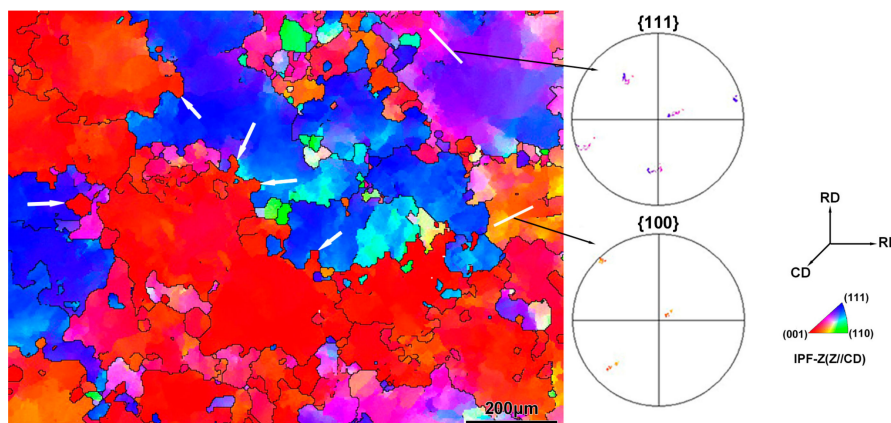

Figure 5. Orientation characterization of recrystallization grain of sample c3: (**a**) orientation distribution map of recrystallized grains with IPF colors; (**b**) {100} and {111} pole figures of the deformed grains; (**c**) {100} and {111} pole figures of the recrystallized grains.

3.4. D-SIBM (Dynamic Strain-Induced Boundary Migration) about <100>-Oriented Grains

Although dynamic recrystallization would occur during hot compression, deformed grains with a highly dynamic recovered state often dominate the evolution of the compressed microstructure. Warchomicka et al. [18] revealed that the main dynamic restoration mechanism is dynamic recovery for the hot compressed Ti55531 alloy at all the deformation parameters. Dynamic recovery could not solely change the deformation texture, and dynamic recrystallization is not enough to change the deformation texture because of its low volume fraction, as discussed in Section 3.2. Strain-induced boundary migration (SIBM) is an important mechanism during the recrystallization of deformed metals [19]. Nucleation would be initiated at the grain boundaries with the SIBM due to different

stored energies and dislocation densities between <100>-oriented grains and <111>-oriented grains. The orientation of new grain may be different than either of the initial grains or be similar to one of the neighboring grains. The stored energy is partially released by dynamic recovery, but is not enough for the nucleation of dynamic recrystallization. The storage energy and dislocation density still remain different between <100>-oriented grains and <111>-oriented grains during hot compression. Primig et al. [15] considered that the <111>-oriented grains have a larger Taylor factor than <100> grains in molybdenum alloy when {101} and {112} slip systems are taken into account for the calculation in bcc (body-centered cubic) metals. As a result, <111>-oriented grains have a higher stored energy during compression. The bcc titanium alloy has the same crystal structure as the molybdenum alloy. Therefore, it provided a driving force for the grain boundary migration from <100>-oriented grains to <111>-oriented grains rather than nucleation in the grain boundary. As a result, the <100>-oriented grains grow and the <111>-oriented grains are gradually merged in a grain growth process during hot compression. Therefore, dynamic strain-induced boundary migration (D-SIBM) is proposed to illustrate the microstructure evolution. D-SIBM is the main mechanism along with deformation and dynamic recovery of the microstructure, which is different than SIBM during static recrystallization. In the case of low strain rate, dislocations are eliminated because of its rapid recovery rate. Orientation mappings have been tested by the EBSD method to observe the dynamic process of the migration from the <100>-oriented grains to <111>-oriented grains during compression as shown in Figure 6. The grains are at an initially deformed state towards <100> and <111> orientations with the reduction of 40%. With increasing deformation, it can be concluded that the orientations of the deformed grains rotate to <111> or <100> orientations from their initial orientations. As a result, orientations of the deformed grains become stable around <100> and <111>. Meanwhile, the grain boundary migrates more markedly from <100>-oriented grains to <111>-oriented grains, as shown with black arrows in Figure 6. A bowed grain boundary is found in the samples with 40% reduction, and D-SIBM mechanism is proven to be the main path for the growth of <100> grains and the decrease in <111> grains. Eventually, the <100>-oriented fiber texture occupies over 80%, and the <111> fiber texture nearly vanishes when the compressing reduction reaches 80%, as shown in Figure 3b.

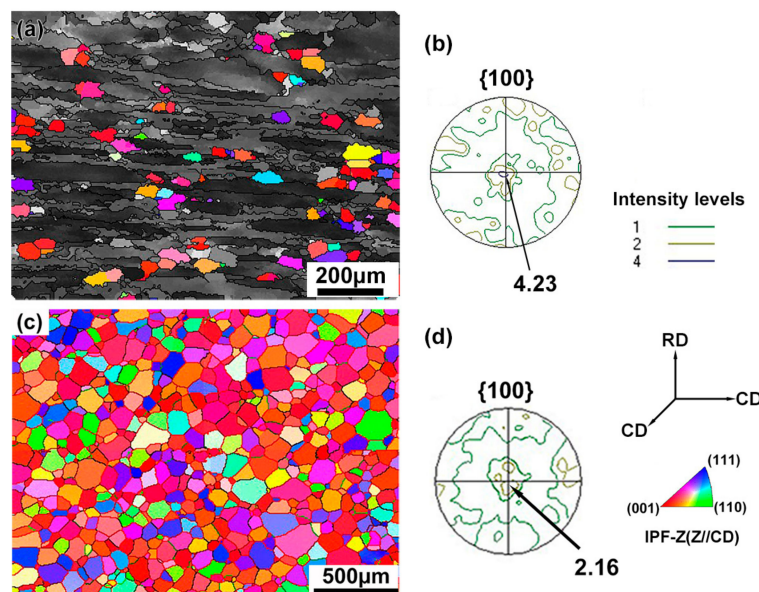
Figure 6. EBSD map with IPF colors of a sample at a strain rate of 0.01 s^{-1} and 40% reductions at 1153 K perpendicular to CD (compressing direction); bowed grain boundaries during migration are shown with white arrows; variation in orientation of deformed grains are shown with {111} and {100} pole figures.

3.5. Recrystallization after Hot Compression

When the compressed sample at a strain rate of 1 s^{-1} is held at the compressing temperature or treated at a low cooling rate, the sample would recrystallize. To study the process of recrystallization, a partially recrystallized microstructure was obtained at a 1 K/s cooling rate after compression, shown in Figure 7a,b. A weak <100> texture was retained for the partial recrystallized grains. The location of

the new grains is almost at the tip of the deformed grains, and can provide more stored energy for recrystallization. The microstructure and texture of the fully recrystallized sample after compression are shown in Figure 7c,d. It can be clearly indicating that the texture of recrystallization is nearly in a random orientation, which is quite different from the deformed texture. Only an extremely weak <100> texture is preserved, because the <100>-oriented grains may be restored to a certain degree during compression. As a result, there is hardly texture inheritance during recrystallization.

The <100> texture is common in a compressed β-titanium alloy, and it is harmful to the mechanical properties because of its large <100>-oriented grains and the low elasticity modulus from the <100> direction. As the mechanism of static recrystallization is different from dynamic recrystallization, texture is also different under the two conditions. Deformation with a relatively high strain rate and static recrystallization during the heat treatment would weaken the deformation texture and refine the grain size.

Figure 7. Orientation maps with IPF colors and {100} pole figure of partial recrystallization and complete recrystallization of the sample cooled by 1 K/s after compression with a reduction of 60% at 1153 K and 1 s^{-1} strain rate; (**a**,**b**) cooled to 1123 K and then water quenched, partial recrystallization; (**c**,**d**) cooled to 1073 K and then water quenched; complete recrystallization; the colored grains are recrystallized grains and the grey grains are deformed grains.

4. Conclusions

(1) Dynamic recrystallization under different parameters during hot deformation was investigated. Low strain rate and large deformation could induce the formation of dynamic recrystallization. Time is a critical factor causing the formation of this type of dynamic recrystallization. The texture after dynamic recrystallization is the <100> fiber texture, similar to the deformed texture.

(2) Dynamic strain-induced boundary migration was discovered during the low strain rate compression and is considered as the main mechanism causing the formation of a strong <100> texture during compression at a high temperature and low strain rate. The increasing temperature and strain rate of hot compression could promote the migration of <100>-oriented grains towards <111>-oriented grains. As a result, the <100> texture would be strengthened and the <111> texture would be weakened.

(3) To control the texture of the BCC titanium alloys, high strain rate and recrystallization after compression should be applied during hot deformation, which would be beneficial to eliminate the strong <100> texture. Nucleation of static recrystallization in the hot-compressed samples

forms at the tip of the deformed <111>-oriented grains in the samples with 1 s^{-1} strain rate because of the inhomogeneous strain inside these grains. The texture after complete recrystallization is a weak <100> texture, close to the random orientation distribution.

Author Contributions: Kai Li and Ping Yang conceived and designed the experiments; Kai Li and Ping Yang performed the experiments and analyzed the data; Kai Li wrote the paper.

Conflicts of Interest: The authors declare no conflict of interest.

References

1. Markovsky, P.E.; Matviychuk, Y.V.; Bondarchuk, V.I. Influence of grain size and crystallographic texture on mechanical behavior of TIMETAL-LCB in metastable β-condition. *Mater. Sci. Eng. A* **2013**, *559*, 782–789.

2. Fan, J.K.; Kou, H.C.; Lai, M.J.; Tang, B.; Chang, H.; Li, J.S. Hot deformation mechanism and microstructure evolution of a new near β titanium alloy. *Mater. Sci. Eng. A* **2013**, *584*, 121–132.

3. Razavi, S.M.J.; Ferro, P.; Berto, F. Fatigue assessment of Ti-6Al-4V circular notched specimens produced by selective laser melting. *Metals* **2017**, *7*, 291. [CrossRef]

4. Raghunathan, S.L.; Dashwood, R.J.; Jackson, M.; Vogel, S.C.; Dye, D. The evolution of microtexture and macrotexture during subtransus forging of Ti-10V-2Fe-3Al. *Mater. Sci. Eng. A* **2008**, *488*, 8–15.

5. Bai, X.F.; Zhao, Y.Q.; Zhang, Y.S.; Zeng, W.D.; Yu, S.; Wang, G. Texture evolution in TLM titanium alloy during uniaxial compression. *Mater. Sci. Eng. A* **2013**, *588*, 29–33.

6. Obasi, G.C.; Fonseca, D.; Quinta, G.; Rugg, D.; Preuss, M. The effect of beta grain coarsening on variant selection and texture evolution in a near-beta Ti alloy. *Mater. Sci. Eng. A* **2013**, *576*, 272–279.

7. Banumathy, S.; Mandal, R.K.; Singh, A.K. Texture and anisotropy of a hot rolled Ti-16Nb alloy. *J. Alloys Compd.* **2010**, *500*, L26–L30.

8. Kou, H.C.; Chen, Y.; Tang, B.; Cui, Y.W.; Sun, F.; Li, J.S.; Xue, X.Y. An experimental study on the mechanism of texture evolution during hot-rolling process in a β titanium alloy. *J. Alloys Compd.* **2014**, *603*, 23–27.

9. Kim, H.Y.; Sasaki, T.; Okutsu, K.; Kim, J.I.; Inamura, T.; Hosoda, H.; Miyazaki, S. Texture and shape memory behavior of Ti-22Nb-6Ta alloy. *Acta Mater.* **2006**, *54*, 423–433.

10. Li, K.; Yang, P. Investigation of microstructure and texture of beta phase in a forged TC18 titanium alloy bar. *Acta Metall. Sin.* **2014**, *50*, 707–714.

11. Wang, K.X.; Zeng, W.D.; Zhao, Y.Q.; Lai, Y.J.; Zhou, Y.G. Dynamic globularization kinetics during hot working of Ti-17 alloy with initial lamellar microstructure. *Mater. Sci. Eng. A* **2010**, *527*, 2559–2566.

12. Hua, K.; Xue, X.Y.; Kou, H.C.; Fan, J.K.; Tang, B.; Li, J.S. Characterization of hot deformation microstructure of a near beta titanium alloy Ti-5553. *J. Alloys Compd.* **2014**, *615*, 531–537.

13. Chen, Y.; Li, J.S.; Tang, B.; Kou, H.C.; Xue, X.Y.; Cui, Y.W. Texture evolution and dynamic recrystallization in a beta titanium alloy during hot-rolling process. *J. Alloys Compd.* **2015**, *618*, 146–152.

14. Li, L.; Luo, J.; Yan, J.J.; Li, M.Q. Dynamic globularization and restoration mechanism of Ti-5Al-2Sn-2Zr-4Mo-4Cr alloy during isothermal compression. *J. Alloys Compd.* **2015**, *622*, 174–183.

15. Primig, S.; Leitner, H.; Knabl, W.; Lorich, A.; Clemens, H.; Stickler, R. Textural evolution during dynamic recovery and static recrystallization of molybdenum. *Metall. Mater. Trans. A* **2012**, *43*, 4794–4805.

16. Wright, S.I.; Nowell, M.M.; Field, D.P. A review of strain analysis using electron backscatter diffraction. *Microsc. Microanal.* **2011**, *17*, 316–329.

17. Biswas, S.; Kim, D.I.; Suwas, S. Asymmetric and symmetric rolling of magnesium: Evolution of microstructure, texture and mechanical properties. *Mater. Sci. Eng. A* **2012**, *550*, 19–30.

18. Warchomicka, F.; Poletti, C.; Stockinger, M. Study of the hot deformation behaviour in Ti-5Al-5Mo-5V-3Cr-1Zr. *Mater. Sci. Eng. A* **2011**, *528*, 8277–8285.

19. Humphreys, F.J.; Hatherly, M. *Recrystallization and Related Annealing Phenomena*, 2nd ed.; Elsevier: Oxford, UK, 2004; pp. 251–257.